DOI: 10.17344/acsi.2022.7601 *Acta Chim. Slov.* **2022,** *69,* 848–862

Scientific paper

Hybrid Polymer Composite of Prussian Red Doped Polythiophene forAdsorptive Wastewater Treatment Application

Mohd Mustafa,[1] Shabnum Bashir,[1] Syed Kazim Moosvi,[2] Mohd. Hanief Najar,[3] Mubashir Hussain Masoodi[4,*] and Masood Ahmad Rizvi[1,*]

[1] *Department of Chemistry, University of Kashmir, Hazratbal Srinagar, 190006, J&K, India.*

[2] *Department of School Education, Government of Jammu and Kashmir, Srinagar, Jammu and Kashmir, India.*

[3] *Department of Chemistry, Government College of Engineering & Technology, Safapora 193504, Jammu and Kashmir, India.*

[4] *Department of Pharmaceutical Sciences, University of Kashmir, Hazratbal Srinagar, 190006, J&K, India.*

* *Corresponding author: E-mail: masoodku2@gmail.com, mubashir@kashmiruniversity.ac.in*

Received: 08-22-2022

Abstract

Coordination compounds as dopants to conducting polymers combine desirable properties of individual components for a synergistic effect. Prussian red (PR) a low spin iron (III) coordination compound was doped in polythiophene (PTP) matrix to explore propensity of this inorganic-organic hybrid composite material towards wastewater treatment. PR doping was observed to improve mechano, thermal, electrical, and photocatalytic attributes of pure PTP. PTP/PR composite characterization was attempted using the powder X-ray diffraction, TEM, TGA, FTIR, BET analysis and UV-Visible spectroscopy. Optimization of adsorption conditions, adsorbent regeneration, adsorption thermodynamics studies of PTP/PR were carried out using malachite green (MG) dye as a model system. Under optimized conditions 92% MG dye adsorption was observed over 20 mg PTP/PR nanocomposite in 20 minutes at pH 7. PTP/PR nanocomposite also demonstrated a complimentary performance with real wastewater samples. Thermodynamic studies indicate spontaneous process with electrostatic attraction as the predominant noncovalent interaction. This study highlights designing catalysts capable of synergistic adsorption and photocatalytic activities for effective wastewater treatment.

Keywords: Adsorption; Malachite Green; Prussian red; Hybrid Material, Nyquist plot; Kinetics; Isotherms

1. Introduction

Water is the most significant substance for living beings, water scarcity is a global problem, and contamination further adds to it. Persistent contaminants from industrial effluents, domestic sewage, and agricultural practices make water unsafe to the aquatic ecosystem as well as human life.[1,2] Dyes as coloring agents have many applications, limiting their usage is practically impossible, and their eventual disperse in the wastewater/environment is inevitable. Synthetic dyes bring toxicity risks as their intermediate metabolites have been identified to be mutagenic, teratogenic, or carcinogenic, posing serious health threats to ecosystems[3] as well as aesthetic concerns. Malachite green is a triaryl methane cationic dye commonly used in pharmaceutics, paper, textile and printing industries. Treatment methods based on ozonation, nano-filtration, reverse osmosis, flocculation, electrochemical, photocatalytic and advanced oxidation processes are *in vogue* for discoloration of colored water contaminants.[4] Among water treatment methods such as advanced-oxidation, filtration, flocculation, coagulation and microbial degradation,[5,6] adsorption based methods owing to their simplicity, non-invasive reactions, broader scale applicability, lower operational cost, good recyclability are interesting environmentally.[7,8] Consequently, adsorption based methods are still desirable for safer and cost effective wastewater treatment application.

Designing adsorbents with good adsorption capacity and selectivity is a major concern for effective adsorption processes. Natural adsorbents, although pleasing, have limitations of selectivity with lower adsorption capacity.[9] Synthetic adsorbents can be desirably tuned for improved results under controlled conditions such as in sewage treatment plants. Among synthetic adsorbents, conducting polymers (CP) having charge distribution over the entire polymeric surface offer many adsorption sites making these attractive materials towards adsorptive removal of water contaminants. CPs are significantly influenced in shape, porosity, charge separation etc. by doping with suitable dopant. A well-engineered conducting polymer composite can desirably improve the adsorption capacity of the pristine conducting polymer.[10] PR was selected as a dopant with the rationale of its good crystallinity, stability over environmental pH range, high charge density, moderate paramagnetism, redox behavior with relatively lower toxicity.[11] Thus in continuation of our interests in applications of transition metal complexes,[12–16] especially as photocatalysts in organic synthesis,[17,18] and as dopants in conducting polymer matrix for electrical and environmental applications,[19–21] herein we envisaged the effect of Prussian red (PR) as a transition metal complex dopant to the polythiophene conducting polymer matrix. We synthesized polythiophene (PTP) Prussian red (PR) nanocomposite PTP/PR to envisage the effect of this versatile dopant on its polymer properties. The effect of PR dopant on the polymer properties indicated an enhancement in the mechano, thermal, electrochemical and photocatalytic descriptors of pure PTP. The comparative studies of PR doping to PTP, relative to other organic dopants, revealed an increase in surface area, electrical conductivity, charge separation dynamics, and electrochemical stability as desirable attributes for sensing, photocatalytic activity, and device fabrication. The observed physicochemical properties of synthesized PTP/PR nanocomposite indicate its suitability as material for environmental applications, which was modelled using malachite green (MG) dye adsorption in aqueous phase. PTP/PR nanocomposite displayed significant adsorptive tendency towards decoloration of samples having up to 100 ppm of MG dye concentration under environmentally viable conditions (pH 6–7). The effect of adsorbent dose, dye concentration, temperature, adsorption time and pH effect were optimized for its development as adsorbent in real time water treatment plant application. The experimental data of MG dye adsorption over PTP/PR nanocomposite was also analyzed for parameters such as: kinetics, adsorption isotherms and thermodynamics. PTP/PR signified good propensity as hybrid material towards adsorptive handle of water treatment. The development of PTP/PR nanocomposite as an effective water treatment nanomaterial via synergistic adsorptive and photocatalytic elimination of MG dye was also established and its further extension to other persistent water contaminants is underway in our laboratory.

2. Experimental

2. 1. Materials

All the reagents used in the study were of analytical grade and procured from Himedia and Merck India. Thiophene was distilled prior to its use. Malachite green (MG), Potassium ferricyanide and anhydrous Ferric chloride were purchased from Merck India. Potassium ferricyanide was ground by ball milling for size reduction to nano dimension (<10 nm).

2. 2. Synthesis of Nanocomposite

The synthesis of PTP/PR nanocomposite was carried out via oxidative polymerization using $FeCl_3$ as oxidant in a nonaqueous medium.[21] In the optimized synthetic procedure,180mL of 0.05 M $FeCl_3$ solution in chloroform solvent were added (dropwise) to a magnetically stirred solution of 0.022 M distilled thiophene monomer (in 70 mL of chloroform). The reaction mixture contained about 1 g of ground PR dopant (Scheme1). The polymerization reaction mixture was continuously stirred for 24 h, followed by filtering and washing the product several times with methanol to remove any oligomers and unreacted impurities. After repeated acetone washings and room temperature drying, the polymer composite was obtained as a brown powder which was subjected to structural characterization.

2. 3. Measurements

The characterization of the synthesized composite was done using analytical methods and spectroscopic techniques. Infrared spectra were obtained over a Bruker Alpha FTIR spectrophotometer in range 4000–500 cm^{-1}. The structural characterization of samples was performed by the powder X-ray diffraction (PXRD) method using a PW3050 diffractometer (CuKα radiations, λ = 1.5418 Å). The particle shape and size of PTP/PR nanocomposite was analyzed using transmission electron microscopy (TEM) measurements performed on Hitachi SU 8000 microscope at an accelerating voltage of 30 kV. For TEM studies the samples were prepared by spin-casting a THF solution of PTP/PR nanocomposite (3mg/L) on copper grids with carbon coating. The thermogravimetric analysis (TGA) of samples was performed on a SEIKO TG/DTA 6200 instrument. Thermal analysis was done from room temperature to 800°C at a heating rate of 10 °C min^{-1} under nitrogen environment. Adsorption measurements were performed using Double Beam Microprocessor UV-VIS Spectrophotometer (Model:LI-2802). Zeta Potential (surface charge) of the adsorbent particles were determined using an Anton Par Particle Size Analyser (Model:Litesizer 500). BET studies for surface area were attained at 77K using BET instrument, Quantachrome Austosorb IQ Station. The specific surface area and pore size distribution was calcu-

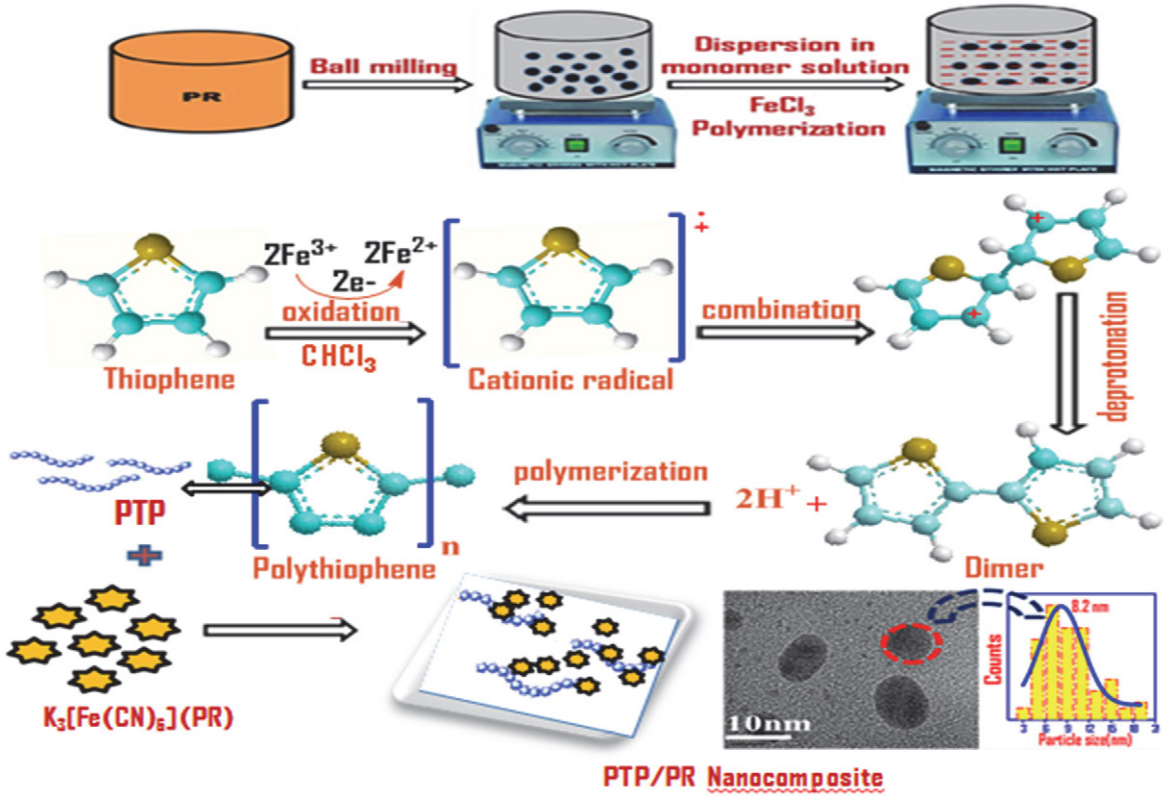

Scheme 1. Schematic depiction of PTP/PR nanocomposite synthesis via $FeCl_3$ oxidative polymerization.

lated using a multiple point BET method and non-local density functional theory (NLDFT) equilibrium model. Electrochemical experiments were carried out on Bio-Logic SAS Potentiostat (Model SP 150) using three electrode system.

2. 4. Adsorption Experiments

For adsorption studies, 20 mg of PTP/PR nanocomposite was added to a 30mL solution of 10ppm MG dye and the suspension was magnetically stirred. Under the optimized reaction conditions, at the regular time intervals aliquots were taken, the adsorbent was separated via centrifugation at 1000 rpm for 20 min and the left-over concentration of dye in the supernatant was measured by a UV–visible spectrophotometer at λ_{max} = 617 nm (corresponding to MG dye). The adsorptive capacity of PTP/PR hybrid material was optimized under influencing parameters like, adsorbent dose, contact time, initial MG dye concentration and temperature range of 25–45 °C. The equations 1, 2 were used to calculate adsorption capacity of PTP/PR nanocomposite and % dye removal efficiency.[22]

$$\text{Adsorption capacity} \quad q = \frac{C_0 - C_t}{m} V \tag{1}$$

$$\%\ Removal = \frac{C_0 - C_t}{C_0} 100 \tag{2}$$

Where, C_0 and C_t (mg/L) are the initial and final (after adsorption) concentrations of MG dye solution respectively, m(g) is the weight of PTP/PR nanocomposite, and V (L) is the initial volume of dye solution.

2. 5. Adsorption Studies of M.G Dye in Real Water Samples

To test the adsorption efficiency of PTH/PR in real samples, the analysis was performed on collected industrial effluent from local textile dye shop (Hazratbal, Srinagar). The dye sample of (1 mg/mL) concentration was prepared in 100 mL deionised water to which required quantities of fixing agent and mordant were also added. To 30 mL of this prepared dye solution 20 mg of PTP/PR composite was added, samples were magnetically stirred and subjected for left over MG dye estimation over different time intervals using UV-visible spectrophotometry. Furthermore, analysis of MG dye adsorption propensity of samples prepared in different water samples (Tap water and deionised water) was also explored under optimized conditions for comparative studies.

2. 6. Cyclic Voltammetry Experiments

The cyclic voltammetry experiments were carried out using three electrode system with Ag/AgCl as reference,

glassy carbon as working, and platinum wire as a counter electrode with 0.1M KNO_3 as supporting electrolyte. The solid samples of PTP/PR and PR each were dispersed in 0.5mL ethanol solution to which 15 µL of nafion was added as binder. The suspensions were kept on ultrasonication for about 30 min to make the slurries of each suspension. The obtained slurries were drop-casted onto glassy carbon electrodes and left for open air drying for 40 min.

3. Results and Discussion

A well-planned dopant to the polymer matrix can generate composites with unique properties for aimed applications. PR turned out to be one such interesting dopant to the polythiophene matrix in terms of modulating essential parameters of a polymer composite system for potential applications. These included enhancement in the mechano, thermal, electrochemical, and photocatalytic attributes of pure PTP. The comparative studies of PR doping to PTP relative to organic dopants revealed an increased surface area, conductivity, and electrochemical stability desirable for electrochemical sensing and device fabrication. The shifting of band gap towards visible region and prevention of charge carrier recombination after PR doping were important attributes for its development as photocatalyst. The synergistic effect of adsorption and photocatalysis was also explored for effective degradation of MG dye.

3. 1. Characterization Analysis

3. 1. 1. IR Spectral Analysis

The FT-IR spectra of synthesized composite were compared with pure reactant forms and are as shown in Figure 1. The broad band around 1630 cm^{-1} and 3300–3400 cm^{-1} is attributed to O-H stretching vibration of adsorbed water on PTP surface, and the range of 600–1500 cm^{-1} reflects the fingerprint region of PTP.[23,24] Furthermore, the C-S stretching vibration of PTP and C-H out of plane deformation modes are designated by weak absorption bands around 690–1300 cm^{-1}. From the Figure 1, the black line corresponding to pure PR shows a specific absorption band around 2100 cm^{-1} that designates CN stretching and the peak at around 600 cm^{-1} is due to Fe-CN vibrations. Moreover, the PTP/PR nanocomposite spectrum exhibits peaks from both the constituents (green line). The intensity of pure PR vibrations is shifted and observed at 2078 cm^{-1} and 497 cm^{-1} in the nanocomposite FT-IR spectrum. Thus, from the peak pattern analysis (shifting of the major stretching frequencies of PTP and PR) the inclusion of PR nanoparticles particles in PTP matrix can be expected.

3. 1. 2. Thermal Analysis

Thermal stability is an essential parameter for material applications, and thermo-gravimetric analysis (TGA) is used to examine this important property via % weight change over the programmed heating. TGA curves of pure PTP and PTP/PR nanocomposite are shown in Figure 2. It is evident from TGA plots that incorporation of PR into PTP matrix has enhanced its thermal stability noticeably. The 33% enhancement in thermal stability of PTP/PR composite compared to pristine PTP at higher temperature indicates stronger interaction between PR dopant and PTP matrix possibly via noncovalent supramolecular type forces. The observed initial weight loss at a lower temperature in case of PTP/PR composite can be attributed to the evaporation of the solvent and clinging low molecular mass volatile compounds. Furthermore, the improved mechano strength of PTP post PR doping is evident from the less sharp slope of % weight loss with temperature in the PTP/PR TGA plot. At 600°C the amount of weight loss in the case of PTP/PR composite is only 60% compared to almost 100% for pristine PTP. Thus it can be inferred from the thermograms that PR doping introduces interactions between dopant and polymer matrix which modulates the mechanical strength of pristine PTP polymer leading to its enhanced thermal stability. A comparative analysis of the dopant effect on the thermal stability of PTP composites with varied dopants indicates the improved thermal stability in the presence of PR dopant.[25,26] The changes in pure PTP structure and function post PR doping were also analyzed using PXRD, Microscopy, and BET analysis.

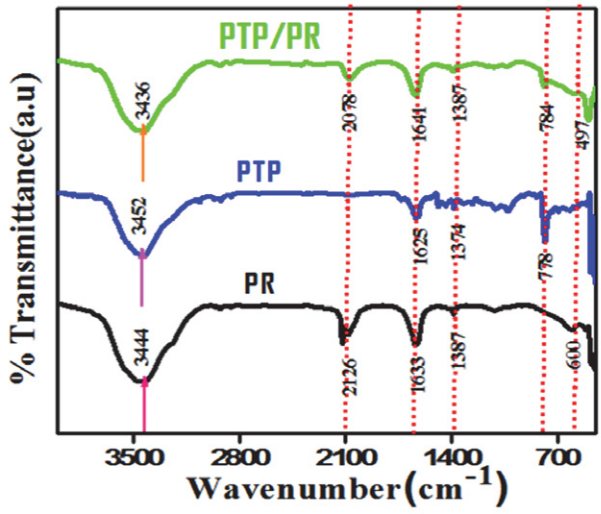

Figure 1. PTP/PR composite characterization (from selected peak picking) using FTIR spectra.

3. 1. 3. XRD Analysis

X-ray Diffraction patterns of PTP and PTP/PR nanocomposite are shown in Figure 3a. Evidently, PTP shows an amorphous halo around Bragg angles of 20–30°, thus exhibiting its amorphous nature.[27] However, the X-ray diffraction pattern of PTP/PR nanocomposite clearly revealed strong intense peaks at various Bragg angles, illus-

trating its crystalline nature. The crystallinity developed in nanocomposite can be attributed to the incorporation of PR in PTP matrix. This corroborates the successful synthesis of prepared nanocomposite, which is also evidenced from TEM micrographs. This is expected as polymers, being larger molecules, are capable of stronger Van der-Waals and other types of possible non-covalent interactions with dopant molecules. These polymer-dopant supra interactions lead to a fair degree of order and compactness in the nanocomposite material.[24] The characteristic peaks were indexed using Powder X software which revealed monoclinic structure with FCC lattice. For crystallite size determination, Scherrer equation (equation 3) has been used.[28–29]

$$D = \frac{k\lambda}{\beta Cos\theta} \quad (3)$$

Where D is the average crystallite size, k the shape factor (0.94), λ the wavelength used (Cu Kα = 1.54 Å), β the FWHM (full width at half maximum) and θ is the Bragg angle. The average crystallite size as determined from above equation has been found to be 7.94 nm. This is almost similar to that obtained from TEM micrographs (8.2 nm), which is indicative of the fact that PR nanoparticle might represent a single grain or crystallite. Thus XRD analysis corroborate with the FT-IR and thermal analysis results.

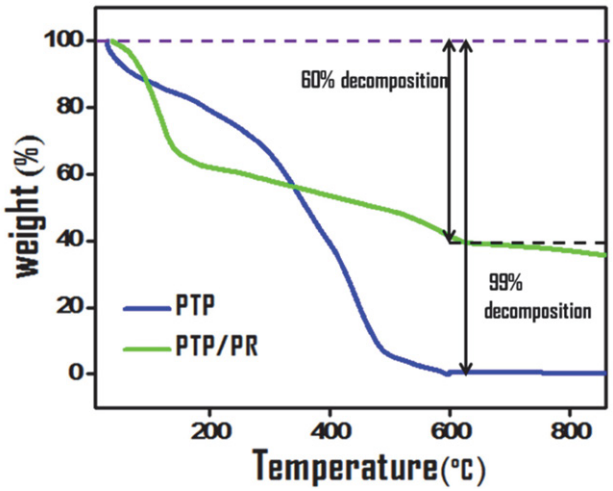

Figure 2. Thermogravimetric analysis plots showing PR enhanced thermal stability of PTP polymer.

3. 1. 4. TEM Analysis

The TEM image of PTP/PR nanocomposite is shown in Figure 3b. The image clearly reveals spherical/granular shape of PR nanoparticles which are dispersed in PTP matrix indicating the formation of nanocomposite. PR nanoparticles are seen to are dispersed in PTP matrix in discrete (inset-1) as well as agglomerated units depending upon their particle size. The agglomeration might result owing to the Van der Waals interaction of smaller particles for bigger sized particles. The particle size distribution of these nanoparticles has been carried out by Image J software followed by Gaussian fitting that revealed the average particle size of around 8.2 nm (inset-2), revealing a mesoporous character. From TEM results, it is clear that PTP/PR is a nanocomposite. Thus, owing to the presence of small sized particles, the nanocomposite is expected to show enhanced surface area, which is confirmed from BET analysis.

3. 1. 5 Structural and Textural Characterization

Adsorption propensity is greatly influenced by the surface area and pore size of the catalyst, BET analysis was attempted to determine surface characteristics of the synthe-

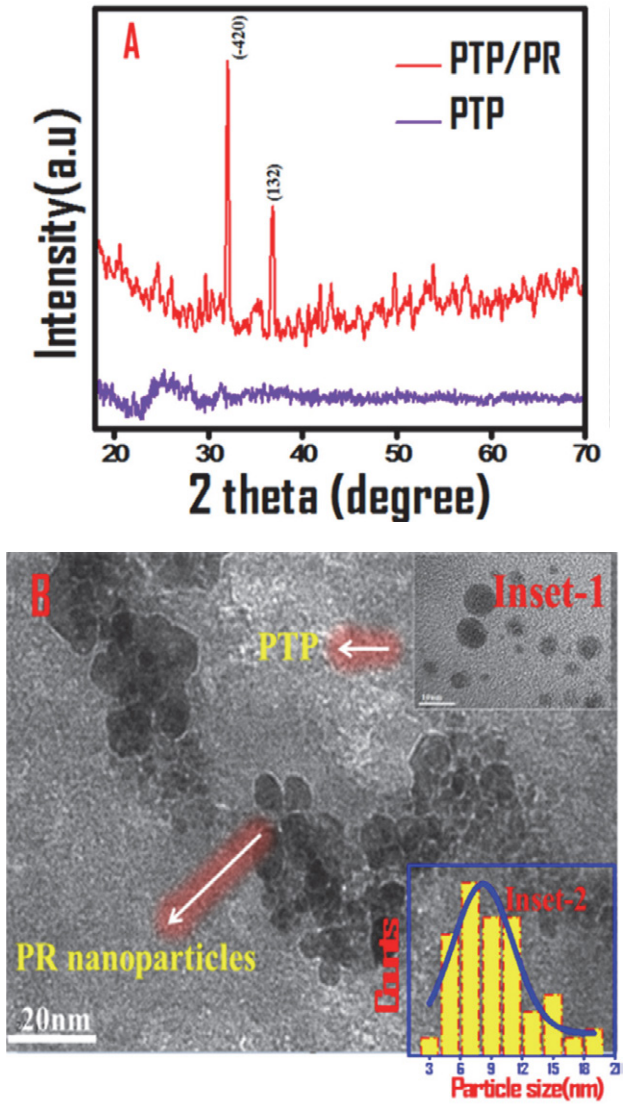

Figure 3. X-ray diffraction pattern of PTP & PTP/PR nanocomposite (A). TEM image of PTP/PR nanocomposite (B) spherical shaped PR nanoparticles of PTP/PR nanocomposite (inset-1). Gaussian histogram fitting plot for particle size distribution (inset-2)

sized PTP/PR nanocomposite. The N_2 adsorption-desorption isotherms and pore diameter distributions of PTP/PR nanocomposite, PR, pure PTP are as shown in Figure 4. The measured surface area for PTP/PR nanocomposite was found to be 81.018 m^2 g^{-1}, which is higher than both PTP (25.560 m^2/g) and PR (15.453 m^2/g) respectively. Besides, the N_2 adsorption/desorption isotherm portrays combined type-II and IV isotherm behavior which is typical of mesoporous structure based on the IUPAC classification.[30,31] Pure PTP has a granular texture with lesser inter-particle distance, which is evident from its lower porosity and smaller surface area. However, on addition of PR, the inter particle space gets increased, which is evident from increased porosity, in case of PTP/PR nanocomposite. The observed increase in porosity can be the reason for the enhanced surface area of PTP/PR nanocomposite compared to undoped PTP.[32] The major pore size distribution of the PTP/PR nanocomposite (2.769 nm) is within the range of 1–3nm, which is a characteristic of smaller pore volume systems. Thus, mesoporous structure with enhanced surface area gives PTP/PR nanocomposite a good adsorptive capacity desirable for an adsorption-based wastewater treatment application. The good surface area and visible region bandgap also makes PTP/PR a possible photocatalyst. The comparative analysis of PTP/PR nanocomposite with other closely related PTP nanocomposite systems indicates a significant increase in surface area for adsorption in case of PTP/PR Table 1.

Table 1. Comparative effect of dopants on the surface area of PTP composites

PTP Composite	Surface area (m^2/g)	Reference
PTP/$Fe(CN)_3(NO)(bpy).4H_2O$	18.9	33
PTP /Fe_3O_4	19.4	27
PTP/Cu	20.88	34
PTP/$CuFe_2O_4$	30.9	35
PTP/PR	81.018	Present work

3. 2. Modeling Adsorptive Propensity of PTP/PR Towards Industrial Dye Malachite Green (MG)

The higher surface area coupled with negative zeta potential value around pH 7 range indicates selectivity of PTP/PR nanocomposite towards cationic water contaminants. With this rationale, we used Malachite green as a model cationic dye for exploring the adsorptive propensity of PTP/PR nanocomposite under environmentally viable conditions.

3. 2. 1. Effects of Contact Time and Initial MG Solution Concentration

The effects of initial MG dye concentration and its contact time on PTP/PR nanocomposite adsorption capacity were observed around 20°C ± 2°C under fixed pH and MG dye concentrations from 10 to 30 mg/L. The adsorption capacity of MG dye on PTP/PR nanocomposite under different initial concentrations with contact time is shown in Figure S1a. At lower dye concentrations, the removal rate was relatively fast and equilibrium was reached within 20 min. which shifted to 25 min. at higher concentrations. The adsorption rate was high for first 20 min. and then progressively saturated with increasing contact time (after 60 min). This observation can be corroborated with the progressive saturation of the available surface sites with increasing contact time. Since many of the adsorption sites get occupied initially and as process proceeds the number of vacant sites gets decreased and occupying remaining sites becomes difficult to occupy due to repulsive forces between the adsorbate molecules on the surface and bulk phases.[22] The effect of initial concentration of MG dye on equilibrium adsorption capacity is shown in Figure S1b. From Figure S1b it can be seen that the equilibrium capacities of MG dye under different initial concentrations showed an increasing trend from 14.187 to 34.5 mg/g signifying that MG dye concentration gradient offers a stronger driving force to reduce the mass transfer resistance of the MG dye. The removal efficiency of MG by PTP/PR displayed relatively higher % removal at lower concentrations with decreasing trend towards high concentrations. This can be corroborated with the fixed adsorption capacity of the 20 mg of PTP/PR sample. Thus from adsorption capacities and removal efficiency studies, 10mg/L was observed as optimized concentration of MG dye in the subsequent experiments.

3. 2. 2. Effect of Adsorbent Dosage

The effect of PTP/PR nanocomposite dosage on adsorption properties was studied by adding its increasing amounts (10 to 30 mg) to 30mL of 10 mg/L MG dye solution at 298 K with stirring for 160 min. with the corresponding results presented in Figure S2. The removal efficiency of MG dye increases from 93.8 to 95.94% on increasing adsorbent dosage from 10 to 30 mg. This behavior can be attributed to the fact that there are more accessible active adsorption sites for MG dye over increasing adsorbent dosage, which increases its % removal efficiency. However, the adsorption capacity reduces from 28.2 to 9.59 mg/g with increasing PTP/PR dose which can be attributed to the aggregate formation at high concentration.[36] The aggregation of adsorbent particles at their higher concentrations was supported by Dynamic Light Scattering technique. DLS data indicates that with increase in adsorbent dosage, particle diameter increases and is shown in Figure S3. The aggregated particles at higher adsorbent dosage create diffusion resistance for MG dye towards the adsorbent surface, thereby decreasing the adsorption capacity. Thus from adsorbent dosage studies of 10 mg to 30 mg PTP/PR, 20 mg gives 94.58% removal effi-

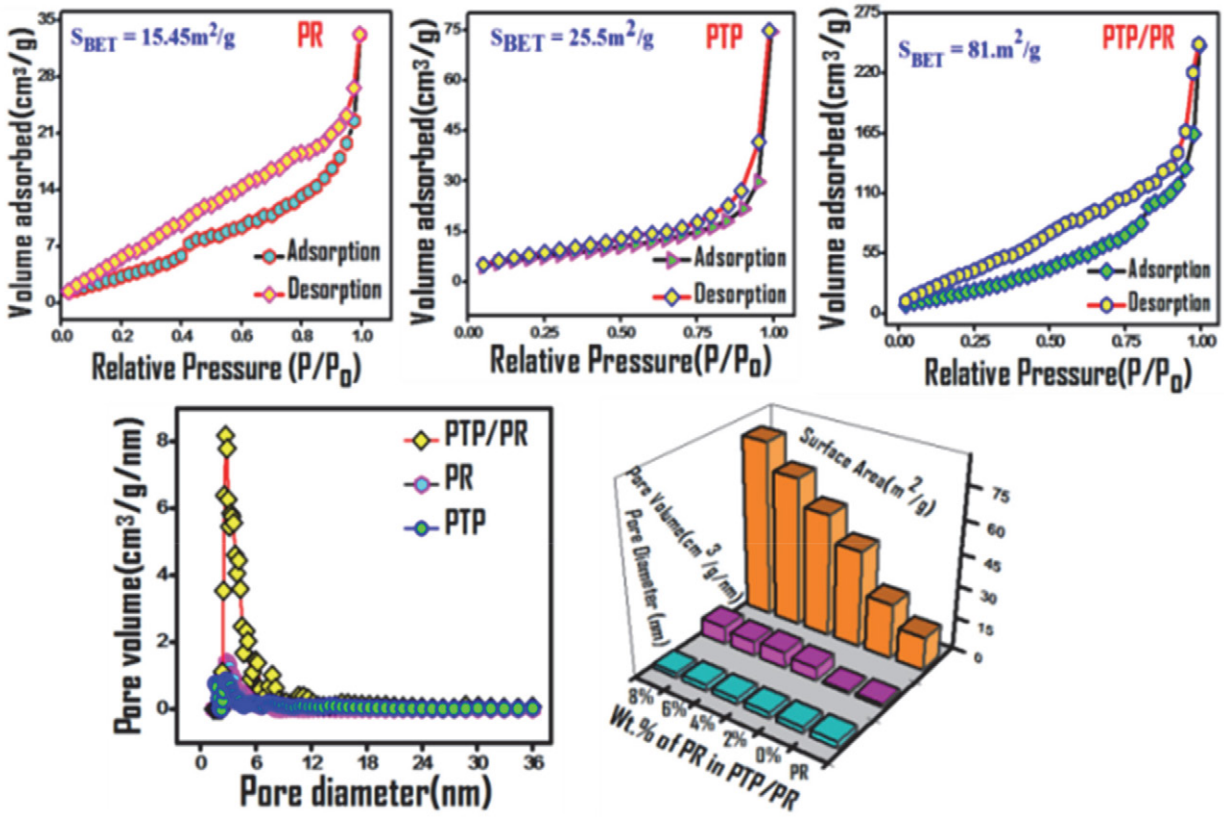

Figure 4. N_2 adsorption-desorption isotherms of PR, PTP and PTP/PR nanocomposite. Pore size distribution curves, Effect of PR wt% on the surface area, pore volume of PTP/PR

ciency under an adsorption capacity of 14.2 mg/g. Further increase in PTP/PR dose was not observed to significantly increase the removal efficiency. Therefore, from the adsorbent dose studies 20 mg was observed as optimum dose for subsequent experiments.

3. 3. Adsorption Kinetic Analysis

Adsorption as a physicochemical process involves the mass transfer of a solute from bulk liquid to the adsorbent surface. Kinetic investigations of such a transfer pave a significant understanding of the adsorption parameters. The kinetics of MG dye adsorption on the PTP/PR nanocomposite was explored by using three kinetic models: pseudo-first-order, pseudo second-order and Elovich models Figure 5 A-C. These kinetic models can be stated in their linear form as equations (4–6). [37,38]

$$\ln(q_e - q_t) = \ln(q_e) - k_1 t \quad (4)$$

$$\frac{t}{q_t} = \frac{1}{k_{2q_e^2}} + \frac{t}{q_e} \quad (5)$$

$$q_t = {}^{1}/_{\beta In\alpha\beta} + {}^{1}/_{\beta Int} \quad (6)$$

where, q_t (mg/g) and q_e (mg/g) are the amounts of MG adsorbed at any time t (min) and at equilibrium, respectively; k_1 (min^{-1}) and k_2 (g/mg/min) are the rate constants of pseudo first order and pseudo-second-order kinetic models respectively. The kinetic parameter counting correlation coefficients (R^2), k_1, k_2 and q_e (cal) values were determined by linear regression. The 'α' in the equation 6 denotes initial adsorption rate (mg/g/min) and 'β' is the desorption constant (g/mg). From the plot of q_t vs lnt, Elovich constants (α, β) were determined from slope and intercept values and the values are presented in Table 2. It is seen from table 2, that the R^2 value (0.9999) for the pseudo-second-order kinetic model was much higher than that of pseudo first-order as well as Elovich kinetic models. In addition, the values of $q_{e,cal}$ calculated under pseudo-second-order model were found close to the experimental $q_{e,exp}$. Based on these observations, the pseudo-second-order kinetic model can be predicted to be the suitable to quantify the adsorption kinetics of MG onto PTP/PR nanocomposite. As is evident from calculated descriptors in table 2, the experimental data do not have an acceptable fitting to pseudo first order and Elovich models. The pseudo second order kinetic model better describes adsorption behavior of MG onto PTP/PR nanocomposite. The pseudo second-order kinetic model broadly involves adsorption, including external film diffusion, intraparticle diffusion and surface adsorption.[22] Typically, intraparticle diffusion is considered as a possible rate-limiting step for a batch

reaction. To envisage the rate-limiting step of the MG dye adsorption process on PTP/PR nanocomposite, the probability of intraparticle diffusion was tested by using Weber–Morris equation 7.[38]

$$q_t = K_{id} t^{0.5} + C \quad (7)$$

Here, K_{id} (mg/g/min$^{-1/2}$) is the intraparticle diffusion rate constant, C (mg/g) is the intercept related to the thickness of the boundary layer. Figure 5D displays the plot of q_t against $t^{0.5}$, and the corresponding kinetic parameters are listed in table S1. It is seen that the regression of q_t versus $t^{0.5}$ was prompted to be linear, and the plots did not pass through the origin, interpreting that besides intraparticle diffusion, film diffusion may also be involved in the rate-controlling step. The Figure 5D shows two stages, an initial stage showing a faster adsorption rate of MG dye from solution, and flat portion depicting decreased adsorption rate due to unavailability of active sites.[39,40] The smaller slope of intra-particle stage than that of the film diffusion stage illustrates lower adsorption is occurring at intra-particle stage.[41] Besides the more significant intercept of the second segment, which gives the thickness of the boundary layer indicates that surface adsorption is also involved in the rate limiting step.[42] Thus, adsorption of MG dye over PTP/PR nanocomposite involves film dispersion and intraparticle diffusion as possible mechanistic processes, with the intraparticle diffusion as a dominant adsorption mechanism.

3. 4. Adsorption Isotherms

In general, adsorption isotherm marks the relationship between the amount of adsorbate adsorbed per unit mass of an adsorbent at a given temperature. Adsorption isotherms are essential descriptors for analyzing and developing any adsorption system.[43] The equilibrium adsorption isotherm unfolds the interaction between the adsorbate and adsorbent. In view of this, MG, PTP/PR system was tested for Langmuir, Freundlich, Temkin isotherm models Figure 6. The Langmuir isotherm model considers monolayer adsorption with all the sorption sites identical and energetically equivalent.[44] The Freundlich isotherm is based on multilayer adsorption on the heterogeneous surface, and there are interactions between the adsorbed molecules.[45]Temkin model considers adsorption on heterogeneous surfaces, effects of indirect adsorbate/adsorbent interactions and assumes heat of adsorption of all molecules decreases linearly with an increase in surface coverage.[44] The linear forms of the three isotherms are given by the following equations (8–10).

$$\frac{1}{q_e} = \frac{1}{q_m} + \frac{1}{K_L q_m C_e} \quad (8)$$

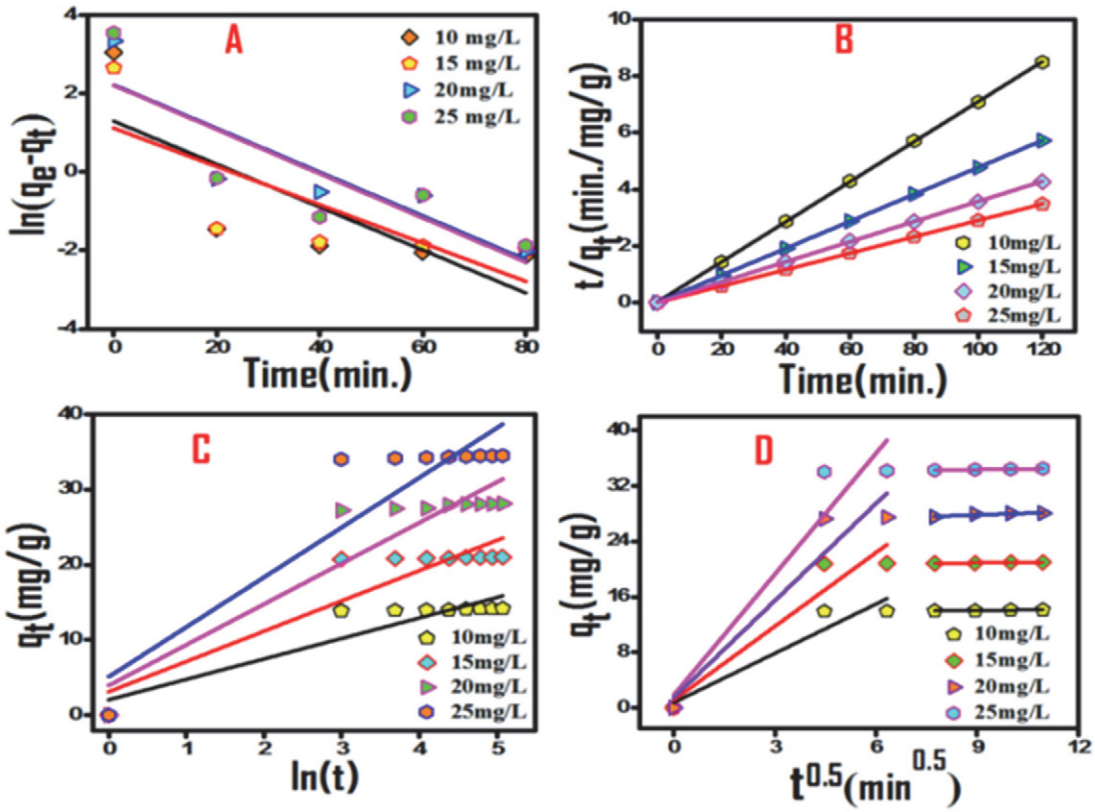

Figure 5. Kinetic models for data fitting of MG (10, 15, 20, 25 mg/L) adsorption onto PTP/PR adsorbent (20mg in 30mL solution at 298K): (A) Pseudo-first order (B) Pseudo-second order (C) Elovich kinetic models (D) Intraparticle diffusion model

Here, q_e (mg/g) is the amount of MG adsorbed at equilibrium time, C_e (mg/L) is equilibrium concentration, q_m (mg/g) is the maximum adsorption capacity and K_L is the Langmuir constant. The parameters of Langmuir model can be calculated from the slope and intercept of the linear plot $1/q_e$ vs $1/C_e$.

$$log(q_e) = log(k_f) + \frac{1}{n} logCe \quad (9)$$

K_F and n are Freundlich constants

$$q_e = \beta ln A_T + \beta ln Ce \quad (10)$$

Where $\beta = RT/b_T$, b_T (kJ/mol) is Temkin constant gives heat of adsorption, T is the absolute temperature (K), R is the universal gas constant (equal to 8.314 J/mol), and A_T is equilibrium binding constant (L/g). The value of Temkin constant indicates the possible mechanism (physical or chemical adsorption) on the adsorbent surface. If $b_T > 40$ kJ/mol, chemisorption occurs and if $b_T < 40$ kJ/mol, physisorption proceeds.[46] The quantities K_F, K_L, n, q_0, b and qt were calculated, and the values are summarized in Table 3. The correlation coefficient for Langmuir isotherm has been found to be higher (0.997) and the adsorption capacity calculated from Langmuir model (34.48 mg/g) is found to be close to the experimental value of 34.5 mg/g. This suggests that the Langmuir isotherm could well explain the adsorption characteristic of PTP/PR nanocomposite. In addition, the separation factor or equilibrium parameter (R_L) of Langmuir adsorption isotherm, which evaluates the feasibility of adsorption on adsorbent was calculated by equation (11). [47]

$$R_L = \frac{1}{1 + K_L C_0} \quad (11)$$

where, K_L was the Langmuir equilibrium constant and C_0 (mg/L) was the initial MG dye concentration. The value of R_L indicated the type of the isotherm to be either irreversible (R_L=0), favorable (0 < R_L< 1), unfavorable (R_L> 1) or linear (R_L = 1). The calculated value of R_L was found in the range of 0.01 – 0.1 in this study,[48] indicating the adsorption of MG on PTP/ PR is favorable, and as such, it can be a good adsorbent material for MG removal from aqueous solution. In addition, the calculated R^2 value of 0.994, for the Freundlich isotherm model signifies a good degree of fit and the heterogeneity factor (n) was calculated to be 1.304. This also confirms a conducive adsorption processes as a reaction is classified as favorable if 1 < n < 10.[49] The fitting of observed adsorption data with regression values of $R^2 > 0.99$ to both Langmuir and Freundlich isotherms models indicate that adsorption of MG dye over PTP/PR nanocomposite includes combined physical as well as chemical adsorption with monolayer/multilayer adsorption.[50,51] The possible forces involved in adsorbate adsorbent interaction include π-π stacking, hydrogen-bond interaction, and electrostatic interaction.

3. 5. Effect of Temperature

To assess effect of temperature on adsorption capacity of PTP/PR nanocomposite for MG, batch adsorption experiments in the temperature range of 25–45 °C were carried out. The adsorption propensity of the PTP/PR nanocomposite improved slightly with increase of system temperature[52,53] (Figure 7A). This can be attributed to increased thermal motion of MG molecules at higher temperature allowing more MG molecules to interact with adsorption sites on PTP/PR nanocomposite. Increasing temperature also decreases viscosity and enhances diffusion of MG dye molecules due to adsorbent surface.[54] An important observation to note was that adsorption capacities of PTP/PR for MG dye remained at relatively high value of above 14.5 mg/g over the entire investigated temperature range, specifying its ability towards MG dye removal under varied temperature conditions.

Table 2. Kinetic models for the adsorption of MG on PTP/PR nanocomposite at 298 K

	Pseudo-1st-order			Pseudo-2nd-order				Elovich model		
C_0 (mg/L)	q_{eexp} (mg/g)	k_1 (min^{-1})	q_{ecal} (mg/g)	R^2	k_2 (g /mg/min)	$q_e$cal (mg/g)	R^2	α (mg/g/min)	β (g/mg)	R^2
10	13.92	0.05	1.042	0.50	0.18	14.14	0.99	7.787	0.368	0.821
15	20.81	0.046	1.218	0.51	0.22	21.28	0.99	22.606	0.248	0.813
20	27.45	0.045	17.95	0.78	0.06	28.17	0.99	51.779	0.185	0.831
25	34.15	0.031	6.184	0.86	0.116	34.5	0.99	164.130	0.151	0.814

Table 3. Isotherm parameters for the adsorption of MG onto PTP/PR nanocomposite at 298 K

Langmuir				Freundlich			Temkin		
K_L(L/mg)	q_m(mg/g)	R_L	R^2	K_f(L/g)	n	R^2	b_T (kJ/mol)	A_T	R^2
1.14	34.48	0.08	0.997	18	1.304	0.994	0.145	12.5	0.98

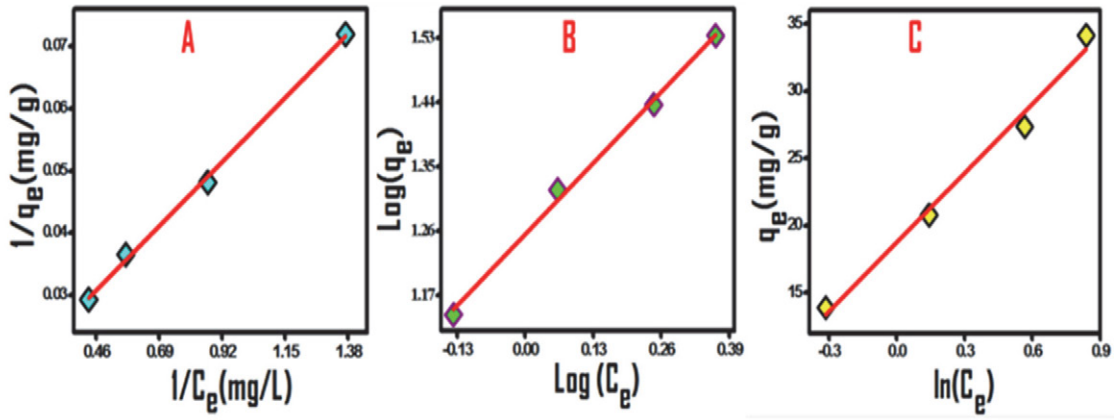

Figure 6. Adsorption isotherms of MG on PTP/PR nanocomposite; (A) Langmuir (B) Freundlich (C) Temkin.

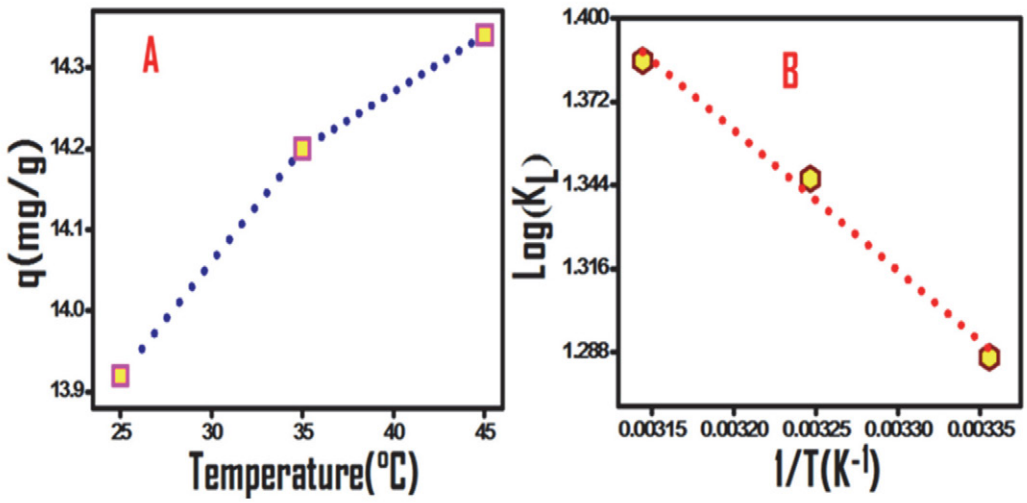

Figure 7 (A) Temperature effect on MG (10 mg/L, 30 mL) adsorption on 20 mg PTP/PR composite (B) Van't Hoff plot

3. 6. Thermodynamic Analysis

The thermodynamic parameters (change in Gibbs free energy (ΔG), enthalpy (ΔH) and entropy (ΔS)) were assessed from the effect of temperature on the adsorption of MG dye onto PTP/PR using the equations (12,13)

$$\Delta G^\circ = -RTln(K_L) \quad (12)$$

$$In(K_L) = -\Delta H^\circ/RT \ + \Delta S^\circ/R \quad (13)$$

where, K_L (L/mol) is the Langmuir equilibrium constant; T(K) is system temperature and R (8.314 J/(mol K)) is the molar gas constant. The negative values of ΔG calculated using equation 12 inferred that adsorption of MG onto PTP/PR nanocomposite is thermodynamically feasible. ΔH and ΔS calculated from slope and intercept of the van't Hoff plot log(K_L) versus 1/T shown in Figure 7B. The calculated thermodynamic parameters of MG dye onto PTP/PR are presented in Table 4. Furthermore, the positive value of ΔH (9.03 kJ/mol) specified that the adsorption process is endothermic in nature. Also, the positive value of ΔS (54.95 J/mol K) means that the randomness increased at the solid–liquid interface during the adsorption of MG dye in the aqueous solution on the PTP/PR nanocomposite.

3. 7. Effect of pH

The pH is a vital parameter to consider adsorptive propensity as it influences surface charge of the adsorbent, degree of ionization of different adsorbates, protonation/deprotonation of functional groups at the adsorbent active sites as well as adsorbate. Moreover, for a significant real time application the adsorption shall occur in the environmentally viable pH range.[55] Accordingly, pH effect for MG dye adsorption on PTP/PR nanocomposite was studied. Figure 8A depicts comparative pH influence towards MG dye adsorption on PTP/PR nanocomposite. Noticeably, adsorption capacities of PTP/PR nanocomposite for MG were relatively higher at pH 7 (14.187 mg/g) and progressively decreased from pH 7 to 4 from 14.187 to 13.53 mg/g. The higher adsorption of MG dye by PTP/PR nanocom-

posite from the neutral solutions was an encouraging result from the wastewater treatment point of view. Under acidic pH, the surface of the PTP/PR gets positively charged due to protonation of sulphur atom of the thiophene units in the polymer matrix,[56] thereby repelling the cationic MG dye from polymer matrix. For pH lower than 7.0, MG dye gradually takes positive charge due to protonation on its nitrogen atoms[57] which decrease adsorption capacities with decreasing solution pH. Around pH 7 deprotonation of sulphur atoms of polymer matrix is complete which attracts cationic MG dye towards PTP/PR surface leading to increased adsorption capacity at environmentally viable neutral pH. The pH effect results were supported by zeta potential studies of PTP/PR nanocomposite over a pH scan Figure 8B. From the zeta potential studies, the pH corresponding to point of zero charge (pHpzc) of pristine PTP[58] and PTP/PR nanocomposite were calculated to be 4.3 and 3.79 respectively. PTP/PR nanocomposite has a point of zero charge (pHpzc) at pH of 3.79 which also marks its transient pH. Above this pH its surface is negatively charged and below it positively charged. The lowered value of pHpzc corroborates with the presence of negative surface charge in case of PTP/PR nanocomposite above pH 3.8. In pH range 0–3 surface of the nanocomposite is expected to have positive zeta potential, which progressively changes with increasing pH and acquires a maximum negative zeta potential value around pH 7 Figure 8B. From zeta potential studies repulsive interaction at lower pH as well as attractive interaction near neutral pH between cationic MG dye and adsorbent surface can hence be confirmed. The negative surface charge under the environmental pH range of 6 to 8 makes, PTP/PR nanocomposite an excellent adsorbent for cationic contaminants in wastewater. The adsorptive propensity of PTP/PR nanocomposite for cationic MG dye prepared in tap, deionized waters and also with anionic dyes was attempted for comparative analysis. Although pH and zeta potential studies indicate dominance of electrostatic interaction for MG dye adsorption onto PTP/PR nanocomposite but the possibility of other interactional forces such as pi–pi stacking and van der Waals type interactions cannot be ruled out.

Table 4. Thermodynamic parameters for adsorption of MG (10 mg/L, 30 mL) onto (20 mg/L) PTP/PR nanocomposite.

T (K)	ΔG° (kJ/mol)	ΔH° (kJ/mol)	ΔS° (J/mol K)
298	–3.194	9.03	54.95
308	–3.446	9.03	54.95
318	–3.663	9.03	54.95

3. 8. Adsorption Mechanism IR Spectrum

To gain some insights about the adsorption mechanism, FTIR spectral analysis of PTP/PR nanocomposite before and after MG dye adsorption was carried out and are as shown in Fig. S4. The FTIR bands of PTP/PR nanocomposite at 490–498 cm^{-1} corresponding to –C-S-C- ring deformation are decreased in intensity and the absorption bands corresponding to –C-H-, -C-C-, O-H stretch get slightly shifted to lower wave numbers post adsorption with MG dye. These changes indicate role of sulphur site -S- in MG dye adsorption process. A prominent absorption band at 2090 cm^{-1} characteristic of -C-N- stretching frequency due to PR particles also gets decreased in intensity after MG dye adsorption indicates ionic type interaction with -C-N-group. Furthermore, the red shift in absorption frequencies can be attributed to electrostatic attraction resulting from lone pair on -S- and cationic MG dye. In addition, pi-pi stacking interaction could be possi-

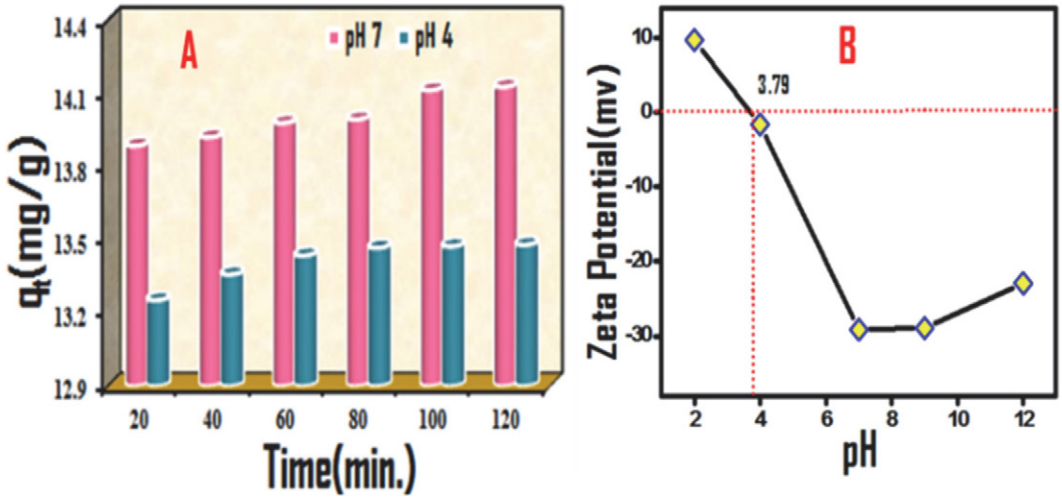

Figure 8. (A) Effects of solution pH on adsorption of MG (10 mg/L, 30 mL) onto the 20 mg of PTP/PR nanocomposite at 298 K.(B) Zeta potential studies of PTP/PR over pH range of 2-12.

ble between aromatic rings of MG dye and polythiophene matrix. The possible adsorption mechanism and probable interactions are shown in Figure S5.

3. 9 Adsorption Studies of MG Dye in Real Time Samples

The real time efficiency of PTP/PR nanocomposite was examined via dye removal efficiency in textile industry wastewater samples. The good adsorptive removal of MG dye from textile industry effluents offers the possibility of using PTP/PR nanocomposite in environmental wastewater treatment application.[59] The efficacy of PTP/PR nanocomposite towards MG dye removal in samples, prepared in normal tap water and deionized water depicted more or less similar % adsorption under optimized conditions Figure 9A. The viability of selective adsorption using PTP/PR were studied by taking Rhodamine as cationic dye, Congo red and Methyl orange as anionic dyes. It was found that the synthesized PTP/PR exhibited higher adsorption capacity towards cationic dyes than anionic dyes Figure 9B. This can be ascribed to the negative surface charge on the PTP/PR nanocomposite under an environmentally viable pH range.

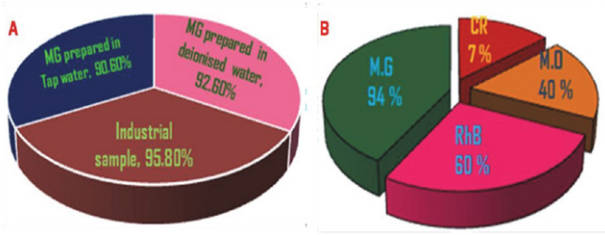

Figure 9. Adsorptive efficiency of PTP/PR towards: (A) real time samples (B) representative dyes from different dye classes.

4. Adsorbent Recovery and Recycling

Adsorption process being a benign and non-invasive method for the widespread wastewater treatment applications is often limited by adsorbent recovery and regeneration post treatment. Regarding regeneration and reusability of adsorbent post treatment, recovery is one of the crucial parameters, magnetic separation is a very helpful method to recover magnetically active adsorbents for an improved economic feasibility. PTP/PR nanocomposite has PR as a magnetic core in the adsorbent nanocomposite, bringing the chances of easy magnetic separation. PTP/PR nanocomposite adsorbent was recovered using magnetic separation any undesired change for better recyclability. In each regeneration cycle, the used adsorbent was suspended in distilled water and magnetically stirred overnight followed by resuspending in 0.1 M HNO_3 and 0.1M NaOH. The adsorption capacity of PTP/PR nanocomposite decreased overall by around 20% after five consecutive cycles post. However, adsorption equilibrium time of 30 minutes progressively increased to 50 minutes after 5 cycles.

4. 1. Synergism of Photocatalysis and Adsorption for Removal of MG Dye by PTP/PR Nanocomposite.

In our attempt to investigate the PR based modulation of the PTP matrix, we calculated the band gap of PTP/PR nanocomposite using Tauc Method.[60] The calculated band gap of 8 wt% of PTP/PR was found to be 2.4 eV relative to the bandgap of 3.0 eV for pure PTP matrix. This PR lowering of band gap has made the PTP/PR nanocomposite as visible light absorbing semiconductor. The larger surface area of 81m^2/g and visible region band gap of PTP/PR nanocomposite are desirable features for the photocatalytic activity. To examine the PR effect on the photo generated hole electron pair recombination of PTP/PR nanocomposite cyclic voltammetry (CV) technique was used. CV experiments in 0.1 M KNO_3 supporting electrolyte at varying scan rates were carried out using PTP/PR nanocomposite and PR modified Glassy carbon electrodes (GCE). The changes in the voltammograms of modified GCE with increasing scan rates from 20 to 100 mV/s can be ascribed to the modified rate of the PR electron transfer in the form of PTP/PR nanocomposite. From Figure 10, it was seen that peak currents increased with scan rate and can be linearly correlated with square root of scan rates suggesting diffusion-controlled process. The shifting of peak potentials on increasing scan rate corroborates with the overall quasi reversibility of redox process. The electrochemical impedance spectroscopy (EIS) analysis of the PTP/PR modified electrode was observed in 0.1M KNO_3. The results of EIS are represented as Nyquist plots depicting semicircular and linear regions. The semicircular part portraying high frequency zone describes electron-transfer resistance (Rct), while the lower frequency linear position indicates diffusion-controlled operation. The higher resistance of PR/GCE electrode can be evidenced from the larger diameter of semicircle which is typically under high Rct condition. The comparatively lower semi-circular arc diameter (Nyquist plot inset of Figure 10) in case of PTP/PR confirms attenuation of Rct on composite formation with PR dopant. The lowering of Rct on composite formation with PTP, indicates that hybrid material (PTP/PR) possesses lower charge transfer resistance indicating that charge carriers (photogenerated electron-hole pairs) are more separated with higher mobility and lower recombination tendency. These attributes are highly desirable for photocatalytic activity.[61]With such desirable properties of PTP/PR nanocomposite towards photocatalytic activity, we envisaged a synergistic effect of photocatalysis and adsorption by PTP/PR nanocomposite towards the MG dye attenuation. The synergistic effect of photocatalysis and

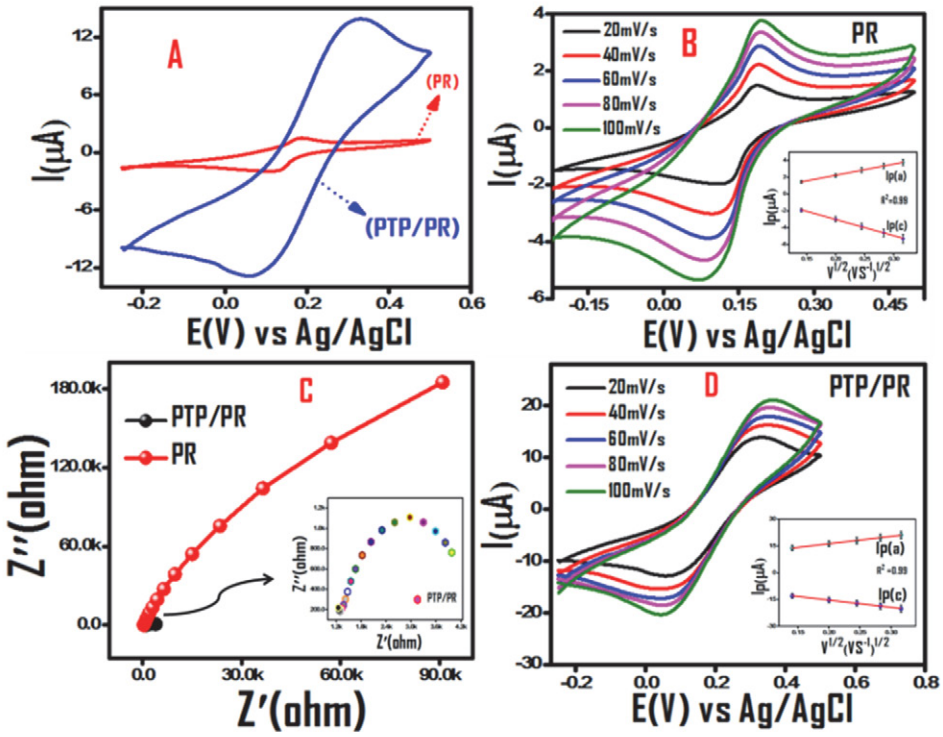

Figure 10. Comparative Cyclic Voltammograms of PR and PTP/PR at constant and increasing scan rates (A, B, D), (C) Comparative Nyquist plots for PR and PTP/PR nanocomposite.

adsorption could be observed within 30 minutes under the irraddiation from 150 W CFL. The results of synergistic effect are summarized in the Fig.11.

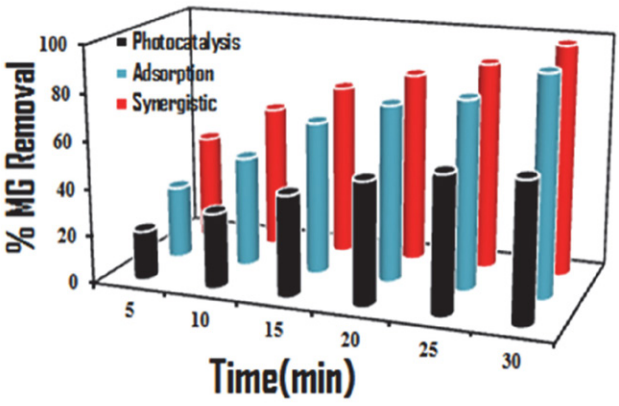

Figure 11. The synergistic effect of photocatalysis and adsorption for MG dye attenuation by PTP/PR nanocomposite

5. Conclusion

Prussian red (PR) on account of its unique properties was envisaged as an inorganic dopant towards polythiophene (PTP) conducting polymer matrix. Oxidative polymerization reaction via solvothermal route was utilized for incorporating ball milled PR in the polythiophene matrix. The interaction of PR with PTP matrix was observed from the spectral changes in the FTIR and PXRD patterns. TEM imaging data identified PTP/PR hybrid material as a nanocomposite system. The observed thermal, electrochemical and photocatalytic descriptors of PTP/PR over pristine PTP suggested a desirable enhancement in these properties for the possible applications as water treatment nano-material. Zeta potential and pH studies suggest good adsorptive propensity towards cationic dyes under environmental conditions. An adsorption capacity of 35mg/g for removal of cationic dye Malachite Green (MG) was observed in the real time effluents from dye industry. From structural analysis, electrostatic, and pi-pi type interactions have been predicted to be predominant noncovalent forces involved in adsorption of MG dye over PTP/PR nanocomposite. Adsorption data fitted Langmuir and Freundlich adsorption isotherms suggesting monolayer as well as multi-layer adsorption process, besides kinetic studies revealed pseudo-second order model for the adsorption of MG dye over nanocomposite. Negative value of free energy indicated thermodynamic spontaneity, recyclability with good regeneration was observed even after five cycles. Taken together PR as novel dopant in the PTP matrix has desirably enhanced its polymeric properties and as PTP/PR nanocomposite, it has increased the potency of conducting polymer towards wastewater treatment application. Further development of PTP/PR nanocomposite for

a wider water treatment application involving combined effect of adsorptive and photocatalytic elimination of persistent water contaminants is underway in our laboratory.

Acknowledgements

The authors are grateful to Head Dept. of Chemistry NIT Srinagar for allowing the BET studies. MM acknowledges the University Grants Commission GOI, for the award of JRF fellowship.

Conflict of interest

The authors declare that they have no conflict of interest and no competing financial interest.

6. References

1. T. H. Y. Lee, J. Chuah, S. A. Snyder, *ACS EST Water* **2022**, *2*, 907–931. **DIO:**10.1021/acsestwater.1c00453
2. W. Ahmad, R. D. Alharthy, M. Zubair, M. Ahmed, A. Hameed, S. Rafque, *Sci. Rep.* **2021**, *11*, 17006. **DIO:**10.1038/s41598-021-94616-4
3. A. Tkaczyk, K. Mitrowska, A. Posyniak, *Sci. Total. Environ.* **2020,** *717,* 137222. **DIO:**10.1016/j.scitotenv.2020.137222
4. R. Al-Tohamy, S. S. Ali, F. Li, K. M. Okasha, A. G. Mahmoud, T. Elsamahy, H. Jiao, Y. Fu, *J. Sun. Ecotoxicol. Environ. Saf.* **2022**, *231*, 113160. **DIO:**10.1016/j.ecoenv.2021.113160
5. Z. Peng, D. Wu, W. Wang, F. Tan, T. Ng, J. Che, X. Qiao, P. Wong. *Appl. Surf. Sci.* **2017**, *396*, 19–25. **DIO:**10.1016/j.apsusc.2016.11.026
6. M. Shaban, M. R. Abukhadra., *Environ. Earth Sci.* **2017**, *76*, 2–16. **DIO:**10.1007/s12665-017-6636-3
7. S. Dutta, B. Gupta, S. K. Srivastava, A. K. Gupta, *Mater. Adv.* **2021**, *2*, 4497. **DIO:**10.1039/D0MA00862A
8. Q. Liu, Y. Li, H. Chen, J. Lu, G. Yu, M. Möslang, J. Y. Zhou. *J. Hazard. Mater.* **2020**, *382*, 121040. **DIO:**10.1016/j.jhazmat.2019.121040
9. I. Custodio, M. Candido, I. Carolina, B. Pires, H. P. Oliveira. CLEAN-SOIL AIR *WATER* **2021**, *49*, 1863–0650. **DOI:**10.1002/clen.202000189
10. J. Stejskal, M. Kohl, M. Trchova, Z. Kolská, M. Pekárek, I. Křivka, J. Prokeš, *Mater. Adv.* **2021**, *2*, 706–717. **DIO:**10.1039/D0MA00730G
11. K. R. Dunbar, R. A. Heintz, *Prog. Inorg. Chem.* **1997**, *45*, 283–391
12. M. A. Rizvi, N. Teshima, G. M. Peerzada, *Croat. Chem. Acta*. **2013**, *86*, 345–350 **DIO:**10.5562/cca2167
13. M. A. Rizvi, S. A. Akhoon, S. R. Maqsood, G. M. Peerzada, *J. Anal. Chem.* **2015**, *70*, 633–638 **DIO:**10.1134/S1061934815050093
14. I. Yousuf, M. Zeeshan, F. Arjmand, M. A. Rizvi, S. Tabassum, *Inorg. Chem. Commun*. **2019**, *106*, 48–53. **DIO:**10.1016/j.inoche.2019.05.027
15. Y. Dangat, M. A. Rizvi, P. Pandey, K. Vanka, *J. Organomet. Chem*. **2016**, *801*, 30–41. **DIO:**10.1016/j.jorganchem.2015.10.015
16. M. A. Rizvi, M. Mane, M. A. Khuroo, G. M. Peerzada, *Monatsh. Chem.* **2017**, *148*, 655–668 **DIO:**10.1007/s00706-016-1813-8
17. M. Kumar, A. Kumar, M. Rizvi, M. Mane, S. C. Taneja, K. Vanka, B. A. Shah, *Eur. J. Org. Chem.* **2014**, 2014, 5247–5255. **DIO:**10.1002/ejoc.201402551
18. S. Devari, M. Kumar, R. Deshidi, M. Rizvi, B. A. Shah, *Beilstein J. Org. Chem.* **2014**, *10*, 2649–2653. **DIO:**10.3762/bjoc.10.277
19. M. A. Rizvi, S. K. Moosvi, T. Jan, S. Bashir, P. Kumar, W. D. Roos, H. C. Swart. *Polymer* **2019**, *163*, 1–12. **DIO:**10.1016/j.polymer.2018.12.044
20. T. Jan, M. A. Rizvi, S. K. Moosvi, M. H. Najar, S. H. Mir, G. M. Peerzada, *ACS Omega* **2021**, *6*, 7413–7421. **DIO:**10.1021/acsomega.0c05799
21. T. Jan, S. K. Moosvi, M. H. Najar, G. M. Peerzada, M. A. Rizvi, *J Mater Sci: Mater Electron* **2022**, *33*, 8179–8192. **DIO:**10.1007/s10854-022-07969-5
22. Q. Xin, J. Fu, Z. Chen, S. Liu, Y. Yan, J. Zhang, Q. Xu., *J. Environ. Chem. Eng.* **2015**, *3*, 1637–1647. **DIO:**10.1016/j.jece.2015.06.012
23. G. Ma, X. Liang, L. Li, R. Qiao, D. Jiang, Y. Ding, H. Chen, *Chemosphere*, **2014**, *100*, 146–151. **DIO:**10.1016/j.chemosphere.2013.11.053
24. M. Faisal, F. A. Harraz, A. E. Al-Salami,S. A. Al-Sayari,A. Al Hajry,M. S. AlAssiri, *Mater. Chem. Phys,* **2018,** *214*, 126-134. **DIO:**10.1016/j.matchemphys.2018.04.085
25. M. Sharif, B. Pourabas, *RSC Adv*. **2016**, *6*, 93680–93693. **DIO:**10.1039/C6RA16701B
26. K. Namsheer, C. S. Rout, *RSC Adv.* **2021**, *11*, 5659–5697. **DIO:**10.1039/D0RA07800J
27. F. Zhanga, Y. Shi, Z. Zhao, W. Song, Y. Cheng, *Appl. Catal. B:Environmental*, **2014,** *150–151,* 472–478 **DOI:**10.1016/j.apcatb.2013.12.049.
28. M. H. Najar, K. Majid,·M. A. Dar, *J. Mat. Sci. Mat. Electron*. **2017**, *28*, 11243–11252. **DIO:**10.1007/s10854-017-6913-7
29. M. H. Najar, K. Majid. *RSC Adv*. **2016**, *6*, 25449–25459. **DIO:**10.1039/C6RA00950F
30. F. Rojas, I. Kornhauser, C. Felipe, J. M. Esparza, S. Cordero, A. Dominguez, J. L. Riccardo, *Phys. Chem. Chem. Phys.* **2002**, *4*, 2346–2355. **DIO:**10.1039/b108785a
31. M. Thommes, K. Kaneko, A. V. Neimark, J. P. Olivier, F. R. Reinoso, J. Rouquerol, K. S. W. Sing, *Pure Appl. Chem.* **2015**, *87*, 1051–1069. **DIO:**10.1515/pac-2014-1117
32. S. P. Takle, S. D. Naik, S. K. Khore, S. A. Ohwal, N. M. Bhujbal, S. L. Landge, B. B. Kale, R. S. Sonawane, *RSC Adv.* **2018**, *8*, 20394. **DIO:**10.1039/C8RA02869A
33. M. H. Najar, K. Majid., *RSC Adv.* **2015**, *5*, 107209–107221. **DIO:**10.1039/C5RA19992A
34. M. Karegar, M. M. Khodaei, *J. Appl. Polym Sci.* **2021**, *139*, 51489. **DIO:**10.1002/app.51489
35. A. H. Kamel, A. A. Hassan, A. E. E. Amr, H. H. El-Shalakany, M. A. Al-Omar, *Nanomaterials* **2020**, *10*, 586. **DIO:**10.3390/nano10030586

36. M. Rajabi, K. Mahanpoor, O. Moradi, *J. Appl. Polym. Sci.* **2019**, *136,* 47495. **DIO:**10.1002/app.47495
37. M. Zhang, L. Chang, Y. Zhao, Z. Yu, *Arab. J. Sci Eng.* **2019**, *44*, 111–121. **DIO:**10.1007/s13369-018-3258-3
38. N. F. Al-Harby, E. F. Albahly, N. A. Mohamed. *Polymers* **2021**, 13, 4446. **DIO:**10.3390/polym13244446
39. R-L. Liu, Y. Liu, X-Y. Zhou, Z-Q. Zhang, J. Zhang, F. Q. Dang, *Bioresour. Technol.* **2014**, *154*, 138–147. **DIO:**10.1016/j.biortech.2013.12.034
40. N. Rajic, D. Stojakovic, D. Jovanovic, N. Z. Logar, M. Mazaj, V. Kaucic, *Appl. Surf. Sci.* **2010**, *257*, 1524–1532. **DIO:**10.1016/j.apsusc.2010.08.090
41. K. Z. Setshedi, M. Bhaumik, S. Songwane, M. S. Onyango, A. Maity, *Chem. Eng. J.* **2013**, *222*, 186–197. **DIO:**10.1016/j.cej.2013.02.061
42. H. K. Boparai, M. Joseph, D. M. O'Carroll, *J. Hazard. Mater.* **2011**, *186*, 458–465. **DIO:**10.1016/j.jhazmat.2010.11.029
43. M. A. A Ghouti, D. A. Da'ana, *J. Hazard. Mater.* **2020**, *393*, 122383. **DIO:**10.1016/j.jhazmat.2020.122383
44. J. Wang, X. Guo, *Chemosphere* **2020**, *258*, 127279. **DIO:**10.1016/j.chemosphere.2020.127279
45. R. Saadi, Z. Saadi, R. Fazaeli, N. E. Fard, *Korean J. Chem. Eng.* **2015**, *32*, 787-799. **DIO:**10.1007/s11814-015-0053-7
46. A. L. Taka, E. F. Kankeu, K. Pillay, X. Y. Mbianda., *Environ. Sci. Pollut. Res.* **2018**, *25*, 21752–21767. **DIO:**10.1007/s11356-018-2055-6
47. S. Pandey, S. B. Mishra, *J. Colloid. Interface Sci.* **2011**, *361*, 509–520. **DIO:**10.1016/j.jcis.2011.05.031
48. J. N. Edokpayi, E. Makete, *Phys. Chem. Earth* **2021**, *123*, 103007. **DIO:**10.1016/j.pce.2021.103007
49. K. Parashar, N. Ballav, S. Debnath, K. Pillay, A. Maity, *J. Colloid. Interface Sci*. **2016**, *476*, 103–118. **DIO:**10.1016/j.jcis.2016.05.013
50. Y. Chen, J. Li, F. Wang, H. Yang, L. Liu, Chemosphere **2021**, 265, 129133. **DIO:**10.1016/j.chemosphere.2020.129133
51. K. Y. Foo, B. H. Hameed, *Chem. Eng. J.* **2010**, *156*, 2–10. **DIO:**10.1016/j.cej.2009.09.013
52. D. Robati, M. Rajabi, O. Moradi, F. Najafi, I. Tyagi, S. Agarwal, V. K. Gupta, *J. Mol. Liq*. **2016**, *214* 259–263. **DIO:**10.1016/j.molliq.2015.12.073
53. K. Gupta, O. P. Khatri, *J. Colloid. Interface Sci.* **2017**, *501*, 11–21. **DIO:**10.1016/j.jcis.2017.04.035
54. C. H. Wu, *J. Hazard. Mater.* **2007**, *144*, 93-100. **DIO:**10.1016/j.jhazmat.2006.09.083
55. M. A. Rizvi, Y. Dangat, T. Shams, K. Z. Khan. *J. Chem. Educ.* **2016**, *93*, 355–361. **DIO:**10.1021/acs.jchemed.5b00499
56. N. C. Joshi, N. Malik, A. Singh. *J. Inorg. Organomet. Polym. Mater*. **2020**, *30*, 1438–1447. **DIO:**10.1007/s10904-019-01252-7
57. G. Y. Abate, A. N. Alene, A. T. Habte, D. M. Getahun. *Environ. Syst. Res.* **2020**, *9*, 29. **DIO:**10.1186/s40068-020-00191-4
58. M. Karegar, M. M. Khodaei, *J. Appl. Polym. Sci.* **2022**, *139*, 51489. **DIO:**10.1002/app.51489
59. S. M. Botsa, K. Basavaiah, *Sci. Rep.* **2020**, 10, 14080. **DIO:**10.1038/s41598-020-70194-9
60. M. M. Abdi, H. N. M. Ekramul Mahmud, L. C. Abdullah, A. Kassim, M. Z. Ab. Rahman, J. L. Ying Chyi, *Chinese J. Polym. Sci.* **2012**, *30*, 93–100. **DIO:**10.1007/s10118-012-1093-7
61. J. Luo, Y. Ma, H. Wang, J. Chen, *Electrochim. Acta* **2015**, *167*, 119–125. **DIO:**10.1016/j.electacta.2015.03.097

Povzetek

Koordinacijske spojine kot dodatki prevodnim polimerom združujejo želene lastnosti posameznih komponent za namen sinergističnega učinka. Koordinacijska spojina prusko rdeča (PR) z železom (III) je bila dopirana v matriko politiofena (PTP) z namenom raziskati nagnjenost tega anorgansko-organskega hibridnega kompozitnega materiala k čiščenju odpadne vode. Dopiranje PR izboljša mehanske, toplotne, električne in fotokatalitske lastnosti čistega PTP. Karakterizacija kompozita PTP/PR je bila opravljena z rentgensko difrakcijo prahu, TEM, TGA, FTIR, BET analizo in UV-vidno spektroskopijo. Optimizacija adsorpcijskih pogojev, regeneracija adsorbenta, študije adsorpcijske termodinamike PTP/PR so bile izvedene z uporabo barvila malahitno zeleno (MG). Pri optimiziranih pogojih je bila dosežena 92% adsorpcija barvila MG pri 20 mg nanokompozita PTP/PR v 20 minutah pri pH 7. Nanokompozit PTP/PR je prav tako dokazal komplementarno učinkovitost v primeru realnih vzorcev odpadne vode. Termodinamične študije kažejo na spontan proces z elektrostatično privlačnostjo kot prevladujočo nekovalentno interakcijo. Raziskava poudarja pomembnost oblikovanja katalizatorjev, ki so sposobni sinergistične adsorpcije in fotokatalitskih aktivnosti za učinkovito čiščenje odpadne vode.